Nonisomorphic Nucleation Pathways Arising from Morphological Transitions of Liquid Channels

H. Kusumaatmaja, R. Lipowsky, C. Jin, R.-C. Mutihac, and H. Riegler

Max Planck Institute of Colloids and Interfaces, Science Park Golm, 14424 Potsdam, Germany
(Received 25 January 2010; revised manuscript received 6 December 2011; published 21 March 2012)

Motivated by unexpected morphologies of the emerging liquid phase (channels, bulges, droplets) at the edge of thin, melting alkane terraces, we propose a new heterogeneous nucleation pathway. The competition between bulk and interfacial energies and the boundary conditions determine the growth and shape of the liquid phase at the edge of the solid alkane terraces. Calculations and experiments reveal a "precritical" shape transition (channel-to-bulges) of the liquid before reaching its critical volume along a putative shape-conserving path. Bulk liquid emerges from the new shape, and, depending on the degree of supersaturation, the new pathway may have two, one, or zero energy barriers. The findings are broadly relevant for many heterogeneous nucleation processes because the novel pathway is induced by common, widespread surface topologies (scratches, steps, etc.).

Introduction.—Phase transitions are influenced by the size or dimensionality of the system because of contributions from interfacial free energies [1,2]. While this has long been known, many details are still poorly understood. Here, we analyze the melting process of such a confined system, the melting of terraced solids. Our findings show for the first time the relevance of morphological instabilities for nucleation processes, in particular, how precritical morphological transitions can lower the nucleation barriers.

Recently, it was shown that the melting of monolayer terraces of long chain alkanes at planar silica-air interfaces [3] leads to moving alkane drops. The drop movement was explained by the wetting properties of the system. However, the emergence of the drops before they start moving has never been investigated. In this Letter, we present new experimental data and analyze for the first time theoretically the onset of the drop formation.

The emergence of the new phase is associated with a nucleation process. Classical nucleation theory [4] shows that for alkanes the critical (heterogeneous) nucleus size is of the order of 100 nm [5]. This is much smaller than the observed drop sizes (microns; see Fig. 1). The question arises of what mechanism leads to the unexpectedly large incipient droplets. We show here that the transition to the macroscopically emerging and growing new phase is critically coupled to a morphological transition or capillary instability from uniform to bulged liquid channels at the terrace edges. The instability provides an energetically favorable pathway for the phase transition. Our theory further predicts that this instability can only occur when the terrace edge length is sufficiently large compared to the edge height. This conjecture is confirmed by experiments on the melting of alkane multilayer island terraces of varying thicknesses.

Apart from addressing the relevance of morphological instabilities for nucleation processes, our Letter shows that surface ledges on the nanometer scale can induce droplets that are orders of magnitude larger, which differs from previous observations of channel-to-droplet instabilities on surface stripes [8]. Long-scale instabilities have been observed in thin layers—see, e.g., [9,10]—but they typically involved external forces, in contrast to the systems studied here.

Our system has rather general properties: (i) melting starts at the edge, (ii) there is a low contact angle of the melt with the surface, and (iii) the contact line is pinned at the terrace edge. It describes widespread situations such as the melting of flat (two-dimensional) solid domains or condensation or adsorption processes on surfaces with terraces, steps, etc. It is also technologically relevant [10–13].

Experimental preparation.—We prepared planar silica surfaces, which were partially covered with large (tens of microns in lateral dimension) contingent areas or terraces
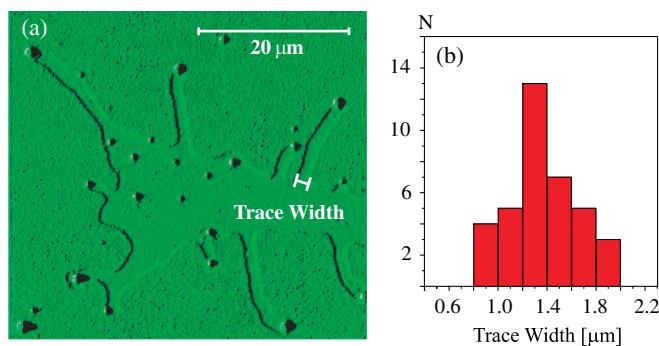

FIG. 1 (color online). (a) Moving alkane droplets appear above the monolayer melting temperature. (b) Histogram of the droplet size. The size of the droplet is equivalent to the trace width.

of uniform thickness that are formed by mono- or multi-layers of solid long chain n-alkanes $C_{36}H_{74}$. The thickness of a solid alkane layer is approximately identical to the molecular all-trans length ($\simeq 4.8$ nm; the molecules are oriented upright [14,15]). For more details on the substrate preparation, see [6,16].

Experimental observation on monolayer melting.—If the temperature is gradually raised above the melting point of the alkane monolayer T_m [17], eventually alkane drops appear at the terrace edges and start to move through the solid monolayer area [18]. The drops have a small contact angle, $\theta \leq 15°$. We focus here on the early stages of the drop formation. We observe that the drops are always already of micrometer size as soon as they appear at the edge (see the supporting movie [16]). This is unexpected because the step is only nanometers high. The drop size is measured via atomic force microscopy by cooling samples with moving drops very quickly, thus freezing the configuration (Fig. 1). The typical width of the orifices of the paths of the drops is $\simeq 1.3$ μm (see the histogram in Fig. 1), about 300 times larger than the height of the terraces.

Theoretical model.—Figure 2(a) shows the geometry of the experimental configuration of the alkane melting from the terrace edge with a step of height h and length $L \gg h$ between the smooth and homogeneous terrace and substrate surfaces. The liquid wets the substrate, rim, and terrace surfaces partially with contact angle θ. The angle α in Fig. 2(a) is a measure of the width of the liquid channel.

The competition between surface and bulk energies determines how much liquid is present at temperature T and which morphology will be formed. The increase in the volume of liquid alkane corresponds to the decrease in the volume of the solid alkane layers (the densities of liquid and solid alkane are approximately equal). Because of interfacial energy contributions and in agreement with
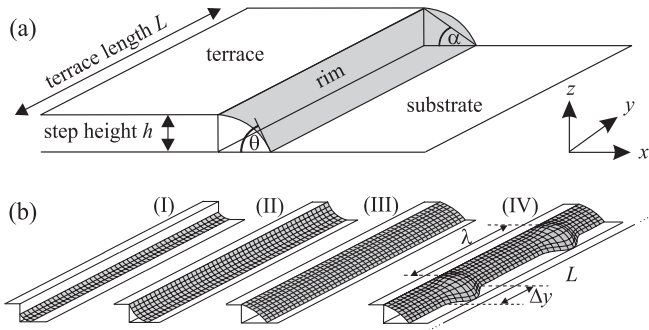
experimental observations, alkane melt will first appear at the terrace ledge. Depending on the liquid volume V, for a given (low) contact angle θ, there are four distinct morphologies [Fig. 2(b)]. (I) A channel with negative curvature at the liquid/vapor surface and an unpinned contact line. (II) Like (I), but with the (left segment) contact line pinned at the terrace edge. (III) A channel with positive curvature, pinned at the terrace edge. (IV) A channel with bulges (localized drops), still pinned at the terrace edge, with a periodic configuration in the y direction (bulge-to-bulge distance $\lambda > \Delta y$, $L = n\lambda$; Δy is the size of the droplet, and n is an integer). The contact line depins when the angle of the liquid with the terrace surface exceeds the equilibrium contact angle.

The interfacial energy of the system can be written as

$$E_I = \Sigma_{LG}A_{LG} - \Sigma_{LG}\cos\theta A_{SL}, \qquad (1)$$

where Σ is the surface tension and A is the area. The subscripts L, G, and S denote liquid, gas, and solid. The relation

$$\Sigma_{LG}\cos\theta = \Sigma_{SG} - \Sigma_{SL} \qquad (2)$$

defines the contact angle θ. Molecular effects are neglected, since, as we shall see later, the size of the resulting droplet is of the order of microns [19].

The interfacial areas of morphologies II and III and the liquid volume are calculated analytically:

$$A_{LG} = \frac{hL}{\sin\alpha}\frac{(\theta - \alpha)}{\sin(\theta - \alpha)}; \qquad A_{SL} = \frac{hL}{\tan\alpha}, \qquad (3)$$

$$V/h^2L = \frac{1}{2\tan\alpha} + \frac{(\theta - \alpha) - \sin(\theta - \alpha)\cos(\theta - \alpha)}{4\sin^2\alpha\sin^2(\theta - \alpha)}. \qquad (4)$$

Substituting Eq. (3) into (1) yields the interfacial energy. To first approximation, we shall assume the terrace length, and thus the surface energy of the vertical ledge, to be constant. For morphology IV, we use a numerical method (Surface Evolver [20]). It minimizes the surface energy of a given volume of liquid with a prescribed geometry. Surface tensions and contact angles are inputs.

Bulk energy contributions, $\Delta\mu V$, result from melting the solid, with $\Delta\mu = \mu_l(T, P) - \mu_s(T, P)$, and $\mu_l(T, P)$ and $\mu_s(T, P)$ are chemical potentials per unit volume in the liquid and solid phases, respectively. We estimate [2]

$$\Delta\mu \simeq -q_m(T - T_m)/T_m, \qquad (5)$$

with q_m the latent heat of melting per unit volume. Positive and negative $\Delta\mu$ correspond to supersaturation of the liquid and solid, respectively.

In the following, we shall use normalized variables $\bar{E} = E/\Sigma_{LG}hL$, $\bar{V} = V/h^2L$, $\bar{P}_L = P_Lh/\Sigma_{LG}$, $\Delta\bar{\mu} = \Delta\mu h/\Sigma_{LG}$, and $\bar{\lambda} = \lambda/h$.

FIG. 2. (a) Schematic diagram of the geometry: θ is the contact angle, and α is the angle between the diagonal and horizontal lines. (b) Possible morphologies for a given contact angle and increasing liquid volume: (I)–(II) a uniform channel with negative curvature, (III) a uniform channel with positive curvature, and (IV) a bulged channel. In (IV), the liquid bulge is not to scale. It is typically much larger.

Coexistence of channel and bulged morphologies.—
Simulations reveal that, for a system as shown in Fig. 2(a),
besides uniform channels, other isocurvature shapes are
possible (i.e., shapes with uniform pressure within the liq-
uid). These shapes are characterized by bulges of equal size
$\Delta \bar{y}$ that are separated by identical channel sections with
distances $\bar{\lambda} > \Delta \bar{y}$; see morphology IV in Fig. 2.

Figure 3(a) shows the normalized interfacial energy of
the system $\bar{E}_I$ as a function of volume $\bar{V}$ for both uniform
and bulged morphologies, respectively ($\theta = 10°$ and $\bar{\lambda} = 1600$, representing our experimental observations). At
small volume, the system is in the uniform channel
morphology. The energy minimum describes a metastable
uniform channel with zero curvature (zero Laplace pres-
sure). With increasing volume, at the minimum, the chan-
nel curvature changes from negative to positive.

At a volume $\bar{V}_{uc}$, the uniform morphology becomes
absolutely unstable and instantaneously transforms into a
bulged morphology (morphology IV, triangles). This tran-
sition at $\bar{V}_{uc}$ is linked to a *jump* in energy. There is also a
lower instability volume $\bar{V}_{bc}$, where, starting in the bulged
shape with $\bar{V} > \bar{V}_{bc}$, upon reducing the volume, the system
will retain its shape until it transforms into a uniform
channel at $\bar{V}_{bc}$. Between $\bar{V}_{uc}$ and $\bar{V}_{bc}$, the system behaves
hysteretically.

Figure 3(b) summarizes the results of calculations as
depicted in Fig. 3(a) for different values of $\bar{\lambda}$ in a morphol-
ogy diagram. It shows regions where (i) only uniform
channels are possible, (ii) both bulges and uniform channels
can exist, and (iii) only bulges are possible. The boundary
between regions (ii) and (iii) also agrees well with an
analytical linear instability analysis [16], which shows
that the lowest volume instability occurs at $\alpha = \theta/2$, i.e.,
at $\bar{V}_{in} = 1/2 \tan(\theta/2) + [\theta/2 - \sin(\theta)/2]/4\sin^4(\theta/2)$, the
volume corresponding to the maximum Laplace pressure
$\bar{P}_L$ of the bulged channel, as we shall see below.

Quite remarkably Fig. 3(b) reveals an absolute lower
limit for $\bar{\lambda}$. For a bulged channel, the quasicylindrical
sleeves of the channel must have the same mean curvature
as the quasispherical bulge. In order to obtain a sphere with
the same mean curvature as a cylinder, the curvature radius
of the sphere must be twice the curvature radius of the
cylinder. Thus, we need a certain minimal size of the bulge
and a certain minimal amount of volume which we can
extract from the quasicylindrical sleeves to form the bulge.
The existence of a $\bar{\lambda}_{min}$ also means melting will proceed
very differently depending on the available normalized
length $\bar{L} = L/h$. Experimentally, this means that the melt-
ing behavior of alkane terraces should depend on their
perimeter L and, respectively, height h. This is indeed
what we observed in Fig. 4 (see also the movies in [16]).
In the first row, $L/h \simeq 200 > \bar{\lambda}_{min}$, and a bulged morphol-
ogy appears. On the other hand, $L/h \simeq 100 < \bar{\lambda}_{min}$ in the
second row, and the system melts in a channel shape. We
note that energy minimization alone favors the formation
of just a single bulge (i.e., $\lambda = L$). However, defects and
dynamical effects may favor the formation of several
droplets. Detailed descriptions of Fig. 4 are given in the
Supplemental Material [16].

The inset in Fig. 3(b) shows the corresponding bulge
size $\Delta \bar{y}$ for a fixed $\bar{\lambda} = 1600$ (other $\bar{\lambda}$ give similar results)
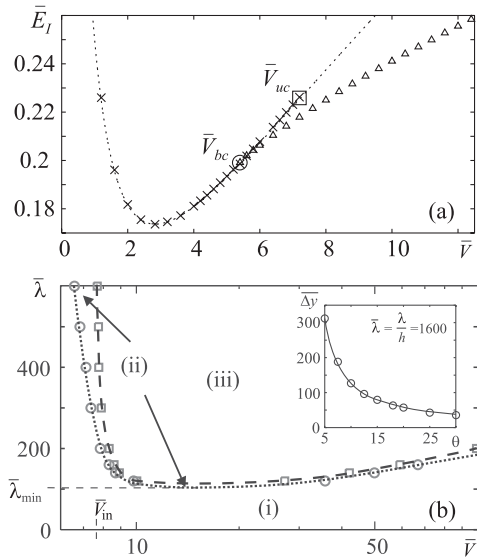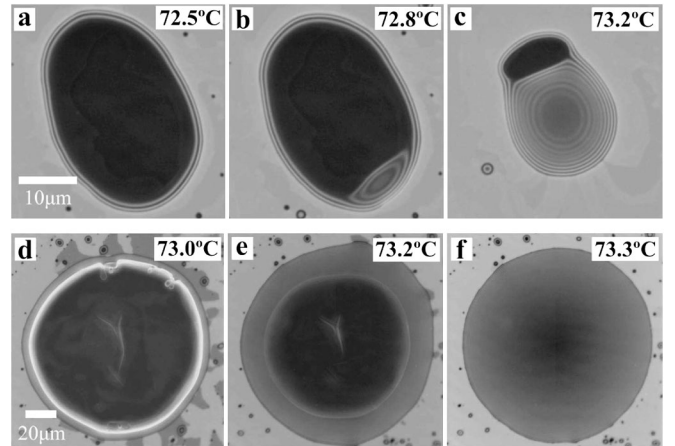

FIG. 3. (a) Interfacial energy as a function of volume for
uniform and bulged morphologies [dashed line = analytical
solution; crosses (uniform) and triangles (bulged) = numerical
results]. Here, we use $\bar{\lambda} = 1600$ and $\theta = 10°$. $\bar{V}_{uc}$ and $\bar{V}_{bc}$ are
instability points for the uniform and bulged morphologies,
respectively. (b) Morphology diagram showing regions where
only (i) uniform channels, (iii) bulges, or (ii) both morphologies
can exist. The inset in (b) shows the bulge/drop dimension
$\Delta \bar{y} = \Delta y/h$ as a function of the contact angle θ.

FIG. 4. Melting behavior of solid alkane terraces with heights
of $\simeq 500$ nm [upper row, (a)–(c)] and $\simeq 4$ μm [lower row, (d)–
(f)]. The 500 nm terrace (a) first grows a liquid channel that (b),
(c) eventually destabilizes into a growing bulge. (d) The $\simeq 4$ μm
terrace also grows a liquid channel. (e) It remains a channel
that (f) eventually converges into a drop without prior bulge
formation.

and various contact angles when the bulge morphologies first become the global minima. $\Delta \bar{y}$ represents the minimum moving drop dimensions because, if the system forms bulged shapes as the temperature increases (as shown below), these bulges will grow in size and eventually become drops. The calculated $\Delta y \simeq 600$ nm for our experimental conditions ($h \simeq 5$ nm, $\theta \simeq 10°$) agrees quite well with the experimentally observed minimum drop size.

Nucleation barrier.—For the nucleation and melting pathway, we need the total energy of the system $\bar{E} = \bar{E}_I + \Delta \bar{\mu} \bar{V}$. Stationary shapes correspond to $d\bar{E}/d\bar{V} = 0$, with $d\bar{E}_I/d\bar{V} = \bar{P}_L$; this means

$$\Delta \bar{\mu} + \bar{P}_L = 0. \qquad (6)$$

For nucleation on a uniform substrate surface, the nucleation pathway is provided by a spherical cap that is isomorphically upscaled. Now, let us consider, for the moment, a corresponding nucleation scenario as obtained by isomorphic upscaling of the uniform channel, a scenario that ignores the morphological instability as illustrated in Fig. 3(a). For the uniform channel, $\bar{P}_L = 2 \sin \alpha \sin(\theta - \alpha)$. $\bar{P}_L$ is plotted in Fig. 5(a) (dashed line). The Laplace pressure has a maximum, $\bar{P}_{L,\mathrm{max}}$, at $\alpha = \theta/2$. This implies [Eq. (6)] a critical temperature, T_{in}, above which there is no energy barrier to complete melting. T_{in} is given by

$$T_{\mathrm{in}} = T_m \left[1 + \frac{2\Sigma_{LG}}{hq_m} \sin^2 \frac{\theta}{2} \right]. \qquad (7)$$

We estimate $T_{\mathrm{in}} - T_m \sim 0.2°$ with typical values for $C_{36}H_{74}$ [5]. Between $0 < \bar{P}_L < \bar{P}_{L,\mathrm{max}}$, there are two channel volumes $\bar{V}$ with the same pressure. Hence, there are two solutions to Eq. (6) for a given supersaturation $\Delta \bar{\mu}$. The solution with the lower $\bar{V}$ corresponds to a local minimum. The larger $\bar{V}$ corresponds to a local maximum. Regarding the nucleation barrier, the larger $\bar{V}$ signifies the peak of the energy barrier for complete melting. The energy barrier for this classical isomorphic nucleation scenario is shown as the dashed line in Fig. 5(b).

The isomorphic nucleation scenario just discussed only applies if the uniform channel does not undergo a morphological transition. In particular, in the situation considered here, a channel with $\bar{\lambda} > \bar{\lambda}_{\mathrm{min}}$ will become unstable due to the morphological (bulging) instability discussed in the preceding section *before* it reaches its critical nucleation volume as a channel. A "*precritical*" morphological transition opens a new and lower energy nucleation pathway. The Laplace pressure of the bulged shapes is plotted in Fig. 5(a) for $\bar{\lambda} = 1600$ (crosses). There are three different regimes of supersaturation. (i) For $-\Delta\bar{\mu} < \bar{P}_{L,bc}$, the nucleation free energy landscape has two barriers. The first barrier corresponds to the upper instability point, at which the uniform channel decays into the bulged channel. This barrier, shown as a dash-dotted line in Fig. 5(b), is not a smooth maximum but instead a sawtooth-shaped discontinuity. The second barrier (solid line) arises from the bulged channel solution. Using the same argument as before, the peak of the barrier corresponds to the solution of Eq. (6) with P_L now the Laplace pressure of the bulged morphology. For small positive $-\Delta\bar{\mu}$, the second barrier is much larger than the first one and dominates the nucleation process. As we increase $-\Delta\bar{\mu}$ towards $\bar{P}_{L,bc}$, the second barrier of the nucleation free energy is reduced and eventually disappears. With increasing λ, the value of $\bar{P}_{L,bc}$ decreases. It is, however, very difficult to numerically determine its asymptotic value. (ii) For $\bar{P}_{L,bc} < -\Delta\bar{\mu} < \bar{P}_{L,uc}$, there is only a single barrier arising from the upper instability point of the uniform channel. This barrier disappears at $-\Delta\bar{\mu} = \bar{P}_{L,uc}$. It is worth noting that, from our linear instability analysis [16], we find in the limit of large $\bar{\lambda}$ that $\bar{P}_{L,uc} \simeq \bar{P}_{L,\mathrm{max}}$. (iii) Finally, the nucleation free energy does not exhibit any barrier for $-\Delta\bar{\mu} > \bar{P}_{L,uc}$.

Discussion and conclusion.—We explain the formation of liquid channels at the edges of alkane terraces, their morphological transformation into bulges, and the observation of unexpectedly large incipient alkane drops. We present a general nucleation and growth scenario for the melting of solid terraces if the liquid melt does not completely wet the surfaces. Promoted by interfacial energy contributions, melting begins already below the bulk melting temperature T_m. The liquid forms a uniform channel whose surface curvatures change from negative to positive when the temperature exceeds T_m. Above T_m, the liquid channel is metastable because the interfacial energy suppresses complete melting. If the uniform channel grew isomorphically, it would reach a certain critical volume corresponding to a maximum of the total energy. Then, the continuously growing bulk phase emerges. We show here for the first time in experiment and theory that, under certain conditions (sufficiently long terrace edges), the growing channel transforms into a bulged morphology *before* it reaches its critical nucleation volume as a channel. This precritical morphological transition opens a new nucleation pathway for the system. Its nucleation barrier is
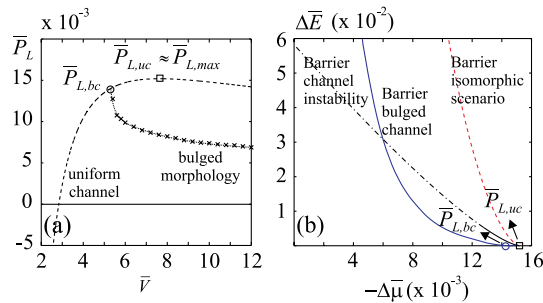

FIG. 5 (color online). (a) Laplace pressure as a function of volume for uniform (dashed line, analytical) and bulged (crosses, Surface Evolver) morphologies. (b) Nucleation energy barriers as a function of supersaturation. $P_{L,uc}$ and $P_{L,bc}$ are the Laplace pressure at the instability points for the uniform and bulged channels.

significantly lower than that obtained by isomorphic upscaling of the uniform channel geometry. This is an important result, since the probabilities to overcome the nucleation barrier typically follow exponential rules $\propto e^{-\Delta E/kT}$. This instability aspect distinguishes our work from previous "multistep" nucleation mechanisms. For example, nucleation pathways with two energy barriers but no shape instabilities have been reported [21]; during the crystallization of silicon, it was shown that the critical (crystalline) nucleus is preceded by the formation of a high-density liquid polymorph [22]. Our investigations further reveal interesting relations between the bulging morphology and the terrace geometry.

Our results are quite general and relevant beyond the melting of alkane terraces. The terrace edge is a paradigm for ubiquitous surface "roughness" topologies, natural or artificial (scratches). The described growth scenario of emerging bulk phases upon melting analogously holds for many condensation, adsorption, precipitation, or deposition processes. It suggests, for instance, that a supersaturated vapor preferentially forms macroscopic liquid drops at a long edge before this happens at a short edge of the same height.

[1] H. K. Christenson, J. Phys. Condens. Matter **13**, R95 (2001).
[2] J. G. Dash et al., Rev. Mod. Phys. **78**, 695 (2006).
[3] P. Lazar and H. Riegler, Phys. Rev. Lett. **95**, 136103 (2005).
[4] D. Kashchiev, Nucleation: Basic Theory with Applications (Butterworth-Heinemann, Oxford, 2000).
[5] $\Sigma_{LG} = 25 \times 10^{-3}$ N/m, $\Delta S = q_m/T_m = 5 \times 10^5$ J/Km^{-3}, $\theta = 10°$, and $\Delta T = T - T_m = 0.2$ K [6,7].
[6] H. Riegler and R. Köhler, Nature Phys. **3**, 890 (2007).
[7] M. Dirand et al., J. Chem. Eng. Data **47**, 115 (2002).
[8] H. Gau et al., Science **283**, 46 (1999).
[9] R. V. Craster and O. K. Matar, Rev. Mod. Phys. **81**, 1131 (2009).
[10] D. Bonn et al., Rev. Mod. Phys. **81**, 739 (2009).
[11] T. M. Squires and S. R. Quake, Rev. Mod. Phys. **77**, 977 (2005).
[12] R. Seemann et al., Proc. Natl. Acad. Sci. U.S.A. **102**, 1848 (2005).
[13] L. Courbin et al., Nature Mater. **6**, 661 (2007).
[14] C. Merkl, T. Pfohl, and H. Riegler, Phys. Rev. Lett. **79**, 4625 (1997).
[15] A. Holzwarth et al., Europhys. Lett. **52**, 653 (2000).
[16] See Supplemental Material at http://link.aps.org/supplemental/10.1103/PhysRevLett.108.126102 for supporting movies, details of our experimental preparation, and linear instability analysis.
[17] Long chain alkanes show surface freezing. The melting point of the first monolayer at the substrate surface is a few degrees higher than the macroscopic bulk melting point [14]. For our purpose, it simply means that the suitable reference melting temperature is the monolayer melting temperature T_m. The described melting scenario is rather general and can be observed for various alkane steps [3].
[18] R. Köhler, P. Lazar, and H. Riegler, Appl. Phys. Lett. **89**, 241906 (2006).
[19] B. Henrich et al., New J. Phys. **10**, 113022 (2008). Using computer simulations, they recently showed that continuum models are adequate for ≥ 2 adjacent fluid monolayers.
[20] K. Brakke, Exp. Math. **1**, 141 (1992).
[21] A. Valencia and R. Lipowsky, Langmuir **20**, 1986 (2004).
[22] C. Desgranges and J. Delhommelle, J. Am. Chem. Soc. **133**, 2872 (2011).